Metabolic Engineering 43 (2017) 147–155

Contents lists available at ScienceDirect

Metabolic Engineering

journal homepage: www.elsevier.com/locate/ymben

Original Research Article

Analysis of mitochondrial metabolism *in situ*: Combining stable isotope labeling with selective permeabilization

Yannic Nonnenmacher[a,b], Roberta Palorini[c], Aymeric Fouquier d'Herouël[b], Lisa Krämer[a,b], Meina Neumann-Schaal[b], Ferdinando Chiaradonna[c], Alexander Skupin[a,d], Andre Wegner[a], Karsten Hiller[a,b,e,*]

[a] Technische Universiät Braunschweig, Department of Bioinfomatics and Biochemistry and Braunschweig Integrated Center of Systems Biology (BRICS), Rebenring 56, 38106 Braunschweig, Germany
[b] Luxemburg Centre for Systems Biomedicine, University of Luxemburg, House of Biomedicine II, L-4367 Belvaux, Luxemburg
[c] Department of Biotechnology and Biosciences, University of Milano-Bicocca, Piazza della Scienza 2, 20126 Milan, Italy
[d] National Centre for Microscopy and Imaging Research, University of California San Diego, 9500 Gilman Drive, La Jolla, CA 92093-0608, USA
[e] Computational Biology of Infection Research, Helmholtz Centre for Infection Research, Inhoffenstraße 7, 38124 Braunschweig, Germany

ARTICLE INFO

Keywords:
Mitochondria
Metabolism
Permeabilization
Stable isotopes
Cancer

ABSTRACT

To date, it is well-established that mitochondrial dysfunction does not only play a vital role in cancer but also in other pathological conditions such as neurodegenerative diseases and inflammation. An important tool for the analysis of cellular metabolism is the application of stable isotope labeled substrates, which allow for the tracing of atoms throughout metabolic networks. While such analyses yield very detailed information about intracellular fluxes, the determination of compartment specific fluxes is far more challenging. Most approaches for the deconvolution of compartmented metabolism use computational models whereas experimental methods are rare. Here, we developed an experimental setup based on selective permeabilization of the cytosolic membrane that allows for the administration of stable isotope labeled substrates directly to mitochondria. We demonstrate how this approach can be used to infer metabolic changes in mitochondria induced by either chemical or genetic perturbations and give an outlook on its potential applications.

1. Introduction

In mammalian cells metabolic reactions are mainly carried out in two different subcellular compartments, *i.e.* the cytosol and the mitochondria. While certain reactions are specific to only one compartment, many metabolic reactions are present in both. This subcellular separation provides the means to adapt mammalian metabolism to changing metabolic needs (Wegner et al., 2015). Compartmentalization enables mammalian cells to carry out reactions that require different conditions, or even forward and reverse reactions at the same time, leading to a largely increased metabolic variability as compared to prokaryotic cells. The complexity of these systems is further increased by the exchange of metabolites between compartments, which also changes dynamically depending on the environmental conditions experienced by the cell (Palmieri and Pierri, 2010). One of the major challenges of modern metabolomics is to deconvolute this metabolic compartmentalization to achieve a better understanding of cellular physiology and thus shed light on the role of metabolism in disease. In recent years, accumulating evidence has shown that mitochondrial dysfunction is closely associated with the emergence and progression of various pathological conditions like cancer, neurodegeneration and inflammation (Krysko et al., 2011; Lin and Beal, 2006; Modica-Napolitano and Singh, 2004). Detailed knowledge of the metabolic adaptations underlying these conditions will help to develop diagnostic tools and unravel potential targets for their treatment and prevention.

On the experimental side, cells are usually cultured under different conditions and metabolites are extracted from the medium and/or the cells. While such analyses yield information about the uptake and secretion rates of different metabolites as well as their intracellular pool sizes, the information on the distribution of intracellular fluxes is limited. To obtain more detailed information on intracellular fluxes, stable isotope labeled substrates can be applied (Klein and Heinzle, 2012; Niedenführ et al., 2015). While most studies use ^{13}C-labeled substrates, the choice of the element to be labeled and its position in

* Corresponding author at: Technische Universiät Braunschweig, Department of Bioinfomatics and Biochemistry and Braunschweig Integrated Center of Systems Biology (BRICS), Rebenring 56, 38106 Braunschweig, Germany.
E-mail address: karsten.hiller@tu-braunschweig.de (K. Hiller).

http://dx.doi.org/10.1016/j.ymben.2016.12.005
Received 1 August 2016; Received in revised form 8 December 2016; Accepted 9 December 2016
Available online 15 December 2016

the molecule strongly depends on the underlying biological question. The corresponding tracers are taken up by the cell and labeled atoms are incorporated into downstream metabolites. The resulting labeling patterns change depending on the activity of different metabolic pathways and thus encode intracellular flux information. Although this approach gives detailed insights into cellular metabolism, subcellular compartmentalization can not be fully resolved. This is due to the fact, that during the extraction of metabolites different pools are collected in one sample and can not be retroactively separated. There are, however, stable isotope labeling approaches that allow for the deconvolution of some compartment specific fluxes based on the application of specific tracers (Lewis et al., 2014). The informative content derived from experimental data can be increased by applying mathematical models that use these data as an input for the computation of intracellular fluxes. To date, ^{13}C-metabolic flux analysis (^{13}C-MFA) represents one of the most promising tools for the estimation of compartment specific fluxes (Antoniewicz, 2015; Wiechert, 2001). However, computed fluxes generally depend on the validity of the underlying model and the applied constraints, and thus, do not necessarily represent the actual state of a cell. Mathematical models rather yield a possible distribution of fluxes that fits to the experimental data within user-defined boundaries. The results obtained from mathematical modeling approaches, therefore, require further experimental testing and either confirmation or rejection of the generated hypotheses.

One approach for the targeted analysis of mitochondrial metabolism is the isolation of mitochondria from cells. Isolated mitochondria are commonly used in studies analyzing oxidative phosphorylation and respiratory activity (Hafner et al., 1990; Holian et al., 1977), but have also been combined with stable isotope labeling (Gravel et al., 2014; Yang et al., 2014). Although this is a well-established and popular technique, there are some drawbacks: the isolation of mitochondria involves many centrifugation steps, takes several hours to perform, and requires a relatively high number of cells (Clayton and Shadel, 2014). Furthermore, isolated mitochondria are removed from their cellular context, rendering them in a less physiological state. A possibility of making mitochondria accessible without isolating them is the selective permeabilization of the cytosolic membrane. This *in situ* state is achieved by treating cultured cells with digitonin, a glycosylated steroid which binds cholesterol with high affinity. Since the cholesterol content of the plasma membrane is around 10-fold higher as compared to the mitochondrial membranes (van Meer et al., 2008), low concentrations of digitonin induce permeabilization of the plasma membrane while leaving mitochondrial membrane integrity unaffected. The resulting *cell ghosts* have been shown to be an appropriate tool for the assessment of mitochondrial metabolite transport and respiratory activity (Nicolae et al., 2015; Wahrheit et al., 2015). In the present study we developed an experimental setup for performing ^{13}C-labeling studies on *in situ* mitochondria of adherent cells and give several examples on how this can be used to assess mitochondrial metabolism.

2. Material and methods

2.1. Cell culture

A549 human adenocarcinoma cells were cultured in Dulbecco's Modified Eagle Medium (DMEM D5796) supplemented with 10% fetal bovine serum (FBS) and 1% Penicillin/Streptomycin. The cells were grown in T75 and T175 flasks (Corning) in a humidified incubator at 37 °C, 5% CO_2 and split 1:5 when reaching 80–90% confluency.

2.2. Pyruvate carboxylase silencing using siRNA

40 pmol of pyruvate carboxylase-targeted or non-targeted siRNA were diluted in 400 OptiMEM medium and mixed gently. After the addition of 5 µl of RNAiMAX, the solution was mixed gently and incubated for 20 min at room temperature. The solution was then added to a well of a 6-well plate. A549 cells (2×10^5) were suspended in 1.6 ml DMEM containing 10% FBS and added to the plate. The mitochondrial assay was performed 48 h after cell seeding.

2.3. Quantitative PCR

RNA was extracted from A549 cells treated with either pyruvate carboxylase-targeted or non-targeted siRNA using the Qiagen RNeasy Kit. Reverse transcription of 600 ng RNA was performed using the SuperScript III reverse transcriptase (Invitrogen) according to the manufacturer's recommendations. Relative quantification of PC cDNA was performed on a Lightcycler 480 (Roche) using cDNA corresponding to 6 ng RNA template, 5 pmol of each forward and reverse primer, and 10 µl iTaq Universal SYBR Green Supermix (Bio-Rad Laboratories). The final volume of the reaction was 20 µl. Initial enzyme activation was performed at 95 °C for 15 min, followed by 40 cycles of denaturation at 95 °C and annealing and elongation at 60 °C for 30 s each.

2.4. Preparation of mitochondrial assay buffer

The mitochondrial assay buffer was derived from different media used in studies on isolated mitochondria and permeabilized cells (Gravel et al., 2014; Salabei et al., 2014; Silva and Oliveira, 2012; Wahrheit et al., 2015). The buffer composition was as follows: 2 mM KH2PO4, 120 mM KCl, 3 mM HEPES and 1 mM EGTA and 3 g/L BSA (essentially fatty-acid free). The pH of the buffer without BSA was adjusted to 7.2 using 5 N KOH. BSA was only added to the buffer on the day of an experiment.

2.5. Mitochondrial assays

A549 cells (2×10^5) were seeded in a 6-well plate and grown for 48 h. The supernatant was removed and cells were washed with 2 ml of PBS. Permeabilization of the cytosolic membrane was induced by incubation with 500 µl digitonin solution (50 µg/ml in mitochondrial assay buffer) for 2 min. Afterwards, cytosolic components were removed by washing three times with mitochondrial assay buffer. Depending on the cell type and the experimental conditions, these washing steps can potentially be omitted. The assay was started by the addition of 1.5 ml of 1 mM glutamine and/or 1 mM pyruvate or their [U-^{13}C] labeled analogue (Cambridge Isotope Laboratories) in mitochondrial assay buffer. The pH of all substrate solutions was re-adjusted to 7.2 using 5 N KOH prior to performing an experiment. After incubation the substrate solution was removed and *cell ghosts* were washed with 2 ml of 0.9% NaCl. Mitochondrial metabolites were extracted by adding 200 µl of each methanol (−20 °C) and dH_2O (4 °C, containing 1 µg/ml D6-glutaric acid as internal standard) and scraping the *cell ghosts* off the plate. The solution was transferred to a tube containing 200 µl chloroform (−20 °C) and agitated for 20 min at 1400 rpm and 4 °C. Polar and non-polar phases were separated by centrifugation (5 min, 21,000×*g*, 4 °C) and 250 µl of the polar phase were transferred to a GC glass vial with microinsert. Samples were dried in a vacuum-centrifuge at −4 °C, capped and stored at −80 °C for subsequent analysis.

2.6. Imaging of mitochondrial membrane potential

A549 cells (5×10^4) were seeded in each compartment of a 35 mm four-compartment glass bottom dish (Greiner CELLview) and grown for 48 h. After staining the cells with 25 nM Tetramethylrhodamine-methyl ester (TMRM) for 30 min they were permeabilized as described in the previous section. To prevent washout of the dye, each solution used during the permeabilization procedure also contained 25 nM TMRM. Glutamine and pyruvate (1 mM each, in mitochondrial assay buffer) were used as substrates during the imaging process. Imaging

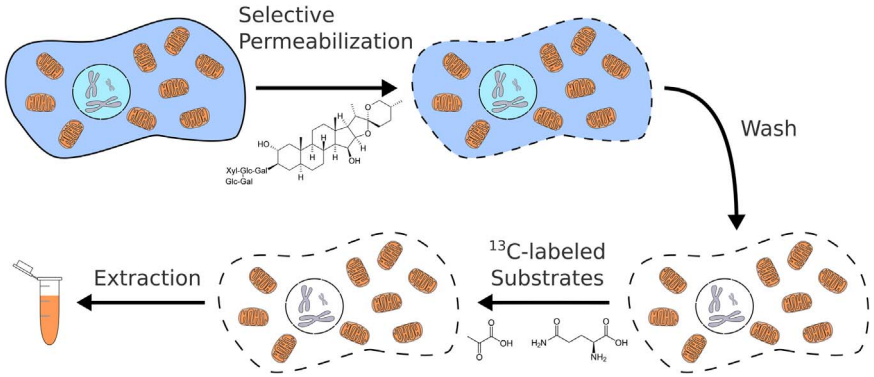

Fig. 1. Schematic workflow of the developed method. Adherent cells are treated with digitonin to induce selective permeabilization and cytosolic components are washed out. The resulting cell ghosts are treated with stable isotope labeled substrates, polar metabolites are extracted and subsequently subjected to GC-MS analysis.

was performed on a Ti-Eclipse epifluorescence microscope (Nikon) with OptoLED light source (Cairn Research) and equipped with a heated enclosure (Solent Scientific) at 37 °C. Cells were imaged using CFI S Plan Fluor ELWD ADM 20X and 40X objectives (Nikon). TMRM emission was acquired using an ET620/60m filter (Chroma) as 16-bit images using an ORCA-Flash4.0 V2 sCMOS camera (Hamamatsu). Relative quantification of TMRM signal was performed using ImageJ. Briefly, color histograms of individual cells were recorded for every timepoint and the signal intensity was calculated using the following formula $\sum_{i=275}^{n} ia_i$, where i represents the color value, n represents the highest color value observed in a sample and a represents the frequency of a color value i in a sample. Data points with a color value lower than 275 were excluded from the calculations to remove background interference. All calculates values were normalized to the first image of the respective timecourse.

2.7. Evaluation of permeabilization efficiency

The optimal digitonin concentration was determined using the LIVE/DEAD Cytotoxicity/Viability Assay Kit (Invitrogen) according to the manufacturer's specifications. Working concentrations for CalceinAM and Ethidium homodimer-1 were 2 µM and 4 µM, respectively. Images were recorded using a Leica DM IL LED fluorescence microscope equipped with a 10x Leica HI Plan objective and a Leica DFC3000 G camera. It should be noted that the optimal digitonin concentration will vary depending on cell type, cell density and assay volume and thus needs to be separately adjusted for each experimental setup.

2.8. GC-MS and data analysis

GC-MS analysis was performed on an Agilent 7890A GC equipped with a 30 m DB-35MS +5 m Duraguard capillary column connected to an Agilent 5975C inert XL MSD. All measurements were carried out in selected ion mode as described previously (Battello et al., 2016). Processing of GC-MS chromatograms and calculation of mass isotopomer distributions was performed using the Metabolite Detector software (Hiller et al., 2009) with chemical formulas taken from a previous publication (Wegner et al., 2014).

2.9. Assessment of mitochondrial respiration

Mitochondrial oxygen consumption rates (OCRs) were determined using a Seahorse XF24 Extracellular Flux Analyzer. A549 cells were seeded in XF plates 24 h prior to the assay. Selective permeabilization was performed immediately before the OCR measurement as described above (75 µg/ml digitonin, 200 µl per well) and the cell ghosts were kept in mitochondrial assay buffer containing no substrates. After equilibration, two measurements of initial OCR were performed followed by two measurements after the following injections (final concentrations are given): 1 mM ADP/10 mM succinate/1 µM rotenone, 1 µg/ml oligomycin, and 1 µM antimycin A.

2.10. Reagents and chemicals

All chemicals were purchased at Sigma-Aldrich, if not stated otherwise.

3. Results and discussion

3.1. Mitochondria in permeabilized cells maintain membrane potential and respiratory activity

Although mitochondrial metabolism has become a field of broad scientific interest, only few experimental tools for its assessment are available. In the current study we present an experimental setup based on the selective permeabilization of adherent cells that allows for the direct administration of substrates to *in situ* mitochondria (Fig. 1). Selective permeabilization of the cytosolic membrane is achieved by the addition of low concentrations of digitonin, which binds cholesterol with both high affinity and specificity. As a result, the integrity of the cholesterol-rich cytosolic membrane is disturbed, whereas the mitochondrial membranes remain mostly unchanged (Fiskum et al., 1980; Schulz, 1990). Similar results can also be obtained by applying other agents, such as saponin or recombinant perfringolysin (Salabei et al., 2014). In combination with stable isotope labeled substrates and a GC-MS based analytical platform this method gives detailed information on metabolic fluxes in mitochondria. In principle the following steps need to be performed: (i) digitonin-induced permeabilization of the cytosolic membrane, (ii) washout of cytosolic components, (iii) incubation of *cell ghosts* with stable isotope labeled substrates under different conditions and (iv) extraction of mitochondrial metabolites.

One of the most important prerequisites when analyzing the function of mitochondria is to ensure their viability and function for the duration of the analysis. Parameters that are commonly related to healthy and active mitochondria are (i) intact membrane potential and (ii) oxidative phosphorylation as measured by means of oxygen consumption. We validated that both of these criteria were met by mitochondria in adherent digitonin-permeabilized cells. We selected the components of the buffer used in this study in order to maintain suitable osmolarity, ionic strength and pH to allow for unconfined mitochondrial function. Media used in mitochondrial studies commonly contain high concentrations of carbohydrates such as sucrose, sorbitol or mannitol. However, we systematically excluded these compounds from the buffer used in this study to prevent interference with the GC-MS analytics.

To determine a suitable concentration of digitonin for this study, we permeabilized A549 cells with different concentrations of digitonin and

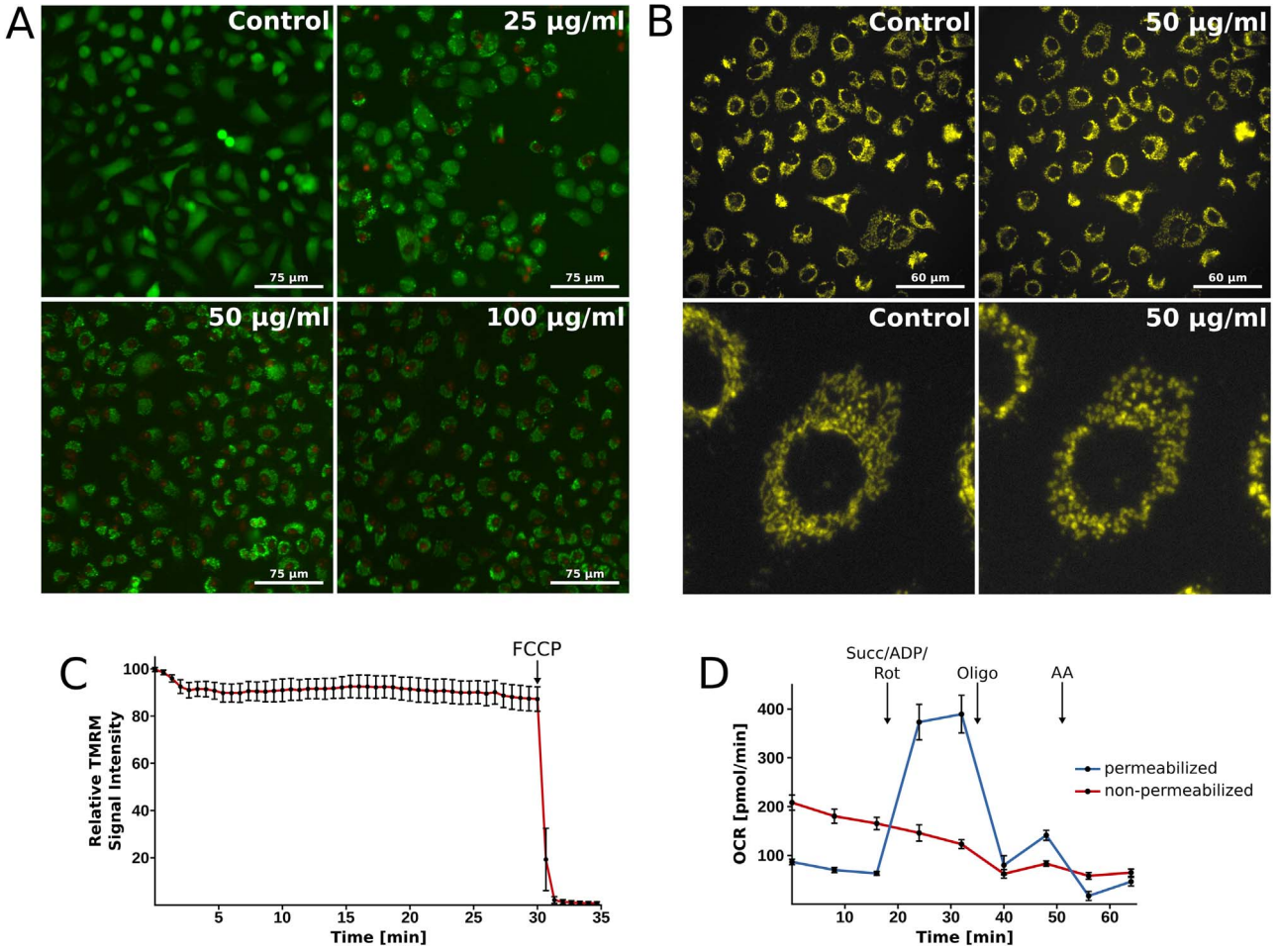

Fig. 2. Live/dead staining, membrane potential and oxygen consumption rate of digitonin-permeabilized cells. (A) Live/dead viability assay of A549 cells permeabilized with different digitonin concentrations. Cells were seeded and cultured as described in Section 2.5 and stained for esterase activity using calcein-AM (green); nuclear DNA of permeabilized cells was stained using ethidium homodimer-1 (red). (B) TMRM staining of A549 cells before and after digitonin permeabilization. The images at the bottom represent magnified sections of the upper images. (C) Relative quantification of the TMRM signal of selectively permeabilized A549 cells over time. FCCP (final concentration: 50 µM) was added at the indicated timepoint. Data points indicate mean values and SD of n=10. (D) Time-resolved OCR of selectively permeabilized and non-permeabilized A549 cells. The following concentrations were used for the indicated perturbations: 10 mM succinate (succ), 1 mM ADP, 1 µM rotenone (rot), 1 µg/ml oligomycin A (oligo) and 1 µM Antimycin A (AA). Data points indicate mean values and SEM of 3 independent measurements with n≥3 each. (For interpretation of the references to color in this figure legend, the reader is referred to the web version of this article.)

performed a live/dead staining (Fig. 2A). In this assay, calcein-AM is taken up by intact cells and cleaved by intracellular esterases to form calcein, which gives rise to a green fluorescence signal. Simultaneously, the DNA binding dye ethidium homodimer-1 (EthD-1) is used to stain the nuclei of cells (red fluorescence signal). Since EthD-1 can, however, not be transported across the cytosolic membrane only the nuclei of permeabilized cells are stained. In non-permeabilized cells we only detected signal from calcein, demonstrating that all cells were intact prior to the digitonin treatment. When permeabilizing the cells with 25 µg/ml digitonin, we observed signal from EthD-1 in a subpopulation of cells, indicating incomplete permeabilization. For concentrations of 50 µg/ml and higher, EthD-1 signal was present in every cell, indicating full permeabilization. Notably, the calcein signal did not disappear in permeabilized cells, but the intracellular distribution of the dye was altered. While in non-permeabilized cells the dye was evenly distributed throughout the whole cell, the signal in digitonin treated cells was only present in subcompartments of the cell. This signal can most likely be ascribed to the uptake and cleavage of the calcein-AM dye by intact mitochondria (Wong et al., 2012). Another criterion that should be considered is that too high concentrations of digitonin are known to permeabilize the outer mitochondrial membrane and cause loss of cytochrome C. We performed a western blot analysis and found that cytochrome C is not released when using 50 µg/ml digitonin in this experimental setup (Suppl. Fig. S1). According to these results, we decided to use 50 µg/ml digitonin for further studies, since this represents the lowest possible concentration that yields full permeabilization without loss of cytochrome C.

To assess how digitonin treatment affects mitochondrial morphology and mitochondrial membrane potential, we performed a staining of A549 cells with the membrane potential-dependent dye Tetramethylrhodamine-methyl ester (TMRM). Fig. 2B shows a TMRM staining of A549 cells before and directly after permeabilization. Prior to the addition of digitonin, mitochondria exhibited a tubular structure and were arranged in a network-like manner. This network-structure was lost upon digitonin treatment, leaving the mitochondria in a more fragmented state. The observed transition was probably caused by the abovementioned disturbance of cellular morphology, since mitochondria are connected to constituents of the cytoskeleton such as microtubules and actin filaments (Heggeness et al., 1978; Manor et al., 2015). Although mitochondrial morphology was altered, the membrane potential remained intact for at least 30 min after permeabilization (Fig. 2C). Addition of the uncoupling agent carbonyl cyanide-*p*-(trifluoromethoxy)phenylhydrazone (FCCP) to mitochondria inside of *cell ghosts* led to a quantitative elimination of membrane potential-dependent TMRM signal. This strongly indicates that the observed signal was indeed caused by an active membrane potential.

As a second indicator of mitochondrial activity we assessed

mitochondrial oxygen consumption *in situ*. We incubated intact and permeabilized A549 cells in mitochondrial assay buffer containing no substrates and sequentially subjected them to different mitochondrial effectors/substrates. Resulting changes in the oxygen consumption rate (OCR) were monitored using a Seahorse XF24 Extracellular Flux Analyzer (Fig. 2D). It should be noted that a higher concentration of digitonin was necessary to archive full permeabilization in the seahorse assay as compared to all other experiments presented in this manuscript. The seahorse assay requires relatively high cell densities in order to give robust and reproducible results and, thus, the concentration of digitonin needed to be adjusted accordingly. We determined the optimal digitonin concentration for this setup by applying different digitonin concentrations in a seahorse run and validated the results using by performing a live/dead staining (Suppl. Figs. S2 and S3).

We observed initial OCRs of 63 and 165 pmol/min for permeabilized and non-permeabilized cells, respectively. Addition of succinate, ADP, and rotenone led to an increase in OCR of the digitonin treated cells to 389 pmol/min. Succinate serves as a direct substrate for complex II (succinate dehydrogenase, SDH) of the electron transport chain (ETC), whereas ADP acts as a phosphate acceptor in the ATP synthase reaction, thus stimulating respiration and in turn electron transport. The complex I inhibitor rotenone is used to prevent the accumulation of oxaloacetate, a potent inhibitor of SDH (Stepanova et al., 2016), and block reverse electron flow from SDH back to complex I (Murphy, 2009). We did not observe an effect on the OCR of the non-permeabilized cells, since both succinate and ADP are not transported across the cytosolic membrane. Subsequent addition of the ATP synthase inhibitor oligomycin A reverses the stimulatory effect of ADP and thus decreased OCR to 80 pmol/min for permeabilized and 62 pmol/min for non-permeabilized cells. The remaining OCR after the addition of oligomycin A is most likely the result of protons leaking across the inner mitochondrial membrane (Abe et al., 2010). Finally, the addition of antimycin A (inhibitor of complex III of the ETC) lowered mitochondrial OCR in permeabilized cells to 17 pmol/min, while we detected only a weak effect on OCR for the intact cells. The observed results are in line with what would be expected for intact and functional isolated mitochondria (Rogers et al., 2011; Yao et al., 2009), demonstrating that the presented setup is well-suited for studies on mitochondrial metabolism.

3.2. Influence of substrate availability on mitochondrial metabolism

To investigate how substrate availability influences mitochondrial metabolic activity we incubated digitonin-permeabilized cells with different substrates. We used pyruvate and glutamine as substrates, because they represent the major energy sources of mitochondria. We applied uniformly ^{13}C-labeled analogues of both compounds to trace their fate through the mitochondrial metabolic network. In contrast to more classical substrates such as glutamate/malate or succinate the application of glutamine and pyruvate allows for a screening of the complete mitochondrial metabolism rather than just parts of it. As a readout for metabolic activity we analyzed the mass isotopomer distribution (MID) of citrate, since in this metabolite pyruvate and glutamine carbon atoms converge.

The application of a [U-^{13}C]pyruvate tracer allows for the assessment of pyruvate dehydrogenase (PDH) and pyruvate carboxylase (PC) activity. PDH activity leads to the formation of fully labeled acetyl-CoA, which can subsequently react with unlabeled oxaloacetate to produce M2 citrate isotopologues (citrate synthase reaction, Fig. 3A). Under conditions with an active PC [U-^{13}C]pyruvate is converted to M3 oxaloacetate which in turn condensates with M2 acetyl-CoA to produce M5 citrate (Fig. 3A). When we added a combination of [U-^{13}C]pyruvate and unlabeled glutamine to digitonin-permeabilized cells, 35% of the mitochondrial citrate pool consisted of M2 citrate isotopologues

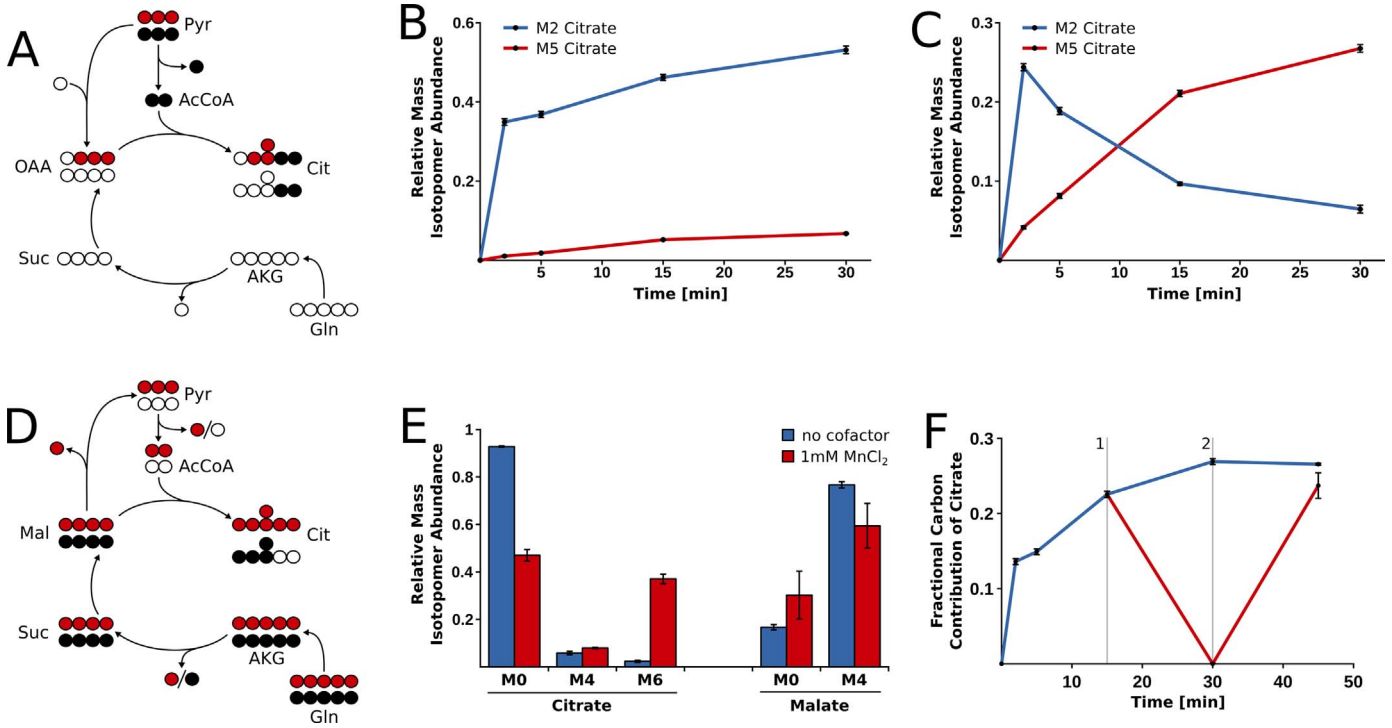

Fig. 3. Influence of substrate availability on A549 mitochondrial enzyme activity *in situ*. (A) Condensed scheme of mitochondrial carbon metabolism with [U-^{13}C]pyruvate and unlabeled glutamine as substrates. (B) Relative abundance of the M2 and M5 citrate isotopologues during incubation with [U-^{13}C]pyruvate and unlabeled glutamine. (C) Relative abundance of the M2 and M5 citrate isotopologues during incubation with [U-^{13}C]pyruvate. (D) Condensed scheme of mitochondrial carbon metabolism with [U-^{13}C]glutamine as substrate. (E) Relative abundance of the M0, M4, and M6 citrate and M0 and M4 malate isotopologues after incubation with [U-^{13}C]glutamine for 15 min. (F) Fractional carbon contribution of [U-^{13}C]pyruvate to citrate. Vertical lines indicate the timepoints at which the substrate was changed from [U-^{13}C]pyruvate to unlabeled pyruvate (1) and back to [U-^{13}C] pyruvate (2, red line). Bars/data points indicate mean values and SD of n=3 for all figures. (For interpretation of the references to color in this figure legend, the reader is referred to the web version of this article.)

already 2 min after substrate addition (Fig. 3B). The M2 abundance steadily increased at a slower rate to ~50% M2 citrate after 30 min. Under these conditions we only observed small amounts of M5 citrate isotopologues (4% after 30 min). In addition, we also observed small quantities of M4 citrate which is produced by metabolic cycling (Suppl. Table S1). In conclusion, these results demonstrate that A549 mitochondria mainly synthesize oxaloacetate from glutamine rather than from pyruvate.

To test, whether mitochondria switch to PC mediated oxaloacetate production when glutamine is not available, we incubated permeabilized A549 cells with [U-^{13}C]pyruvate as the only substrate. Under these conditions only 25% of the citrate pool were M2-labeled after 2 min (Fig. 3C). The M2 fraction then decreased to 6%, whereas the relative abundance of the M5 isotopologue continuously increased to reach 27% after 30 min of incubation. The initial occurrence of the M2 isotopologue indicates the presence of an endogenous pool of TCA cycle metabolites which is still present after permeabilization. This pool supplies the unlabeled oxaloacetate which is necessary for the formation of twofold labeled citrate. However, this pool is expected to be rather small, because the relative abundance of M2 citrate decreases already after two minutes. The emergence of M5 citrate indicates the expected activation of PC. Pyruvate carboxylase is allosterically activated by acetyl-CoA, which accumulates when only little oxaloacetate is available for condensation in the CS reaction (Jitrapakdee et al., 2008). Besides the M2 and M5 citrate we also observed formation of M3, M4 and M6 isotopologues which are formed by cycling (M4 and M6) or condensation of M3 oxaloacetate with unlabeled acetyl-CoA from an endogenous pool (M3, Suppl. Table S2). Taken together we observed that A549 mitochondria use pyruvate as acetyl-CoA source and preferentially use glutamine to synthesize oxaloacetate. Under glutamine limiting conditions however, sufficient oxaloacetate production is ensured by activation of PC.

Similar to the activation of PC under glutamine limiting conditions, we expected an activation of malic enzyme 2 or 3 (ME2/3) under conditions where glutamine is present, but pyruvate supply is limited (Vacanti et al., 2014; Yang et al., 2014). When using a [U-^{13}C] glutamine tracer, oxaloacetate is expected to be labeled at all four carbons (Fig. 3D). In this case, malic enzyme activity then leads to the generation of M3 pyruvate and, subsequently, M2 acetyl-CoA. Condensation of M2 acetyl-CoA with M4 oxaloacetate produces M6 citrate which we used as a readout for ME activity. Surprisingly, only 2% of citrate were M6 labeled after 15 min of incubation with [U-^{13}C] glutamine as the only substrate (Fig. 3E). At the same time 77% of malate were M4 labeled, suggesting only low ME2/3 activity rather than a shortcoming in the metabolic pathway leading from glutamine to malate. Since numerous studies have shown that divalent metal ions such as Mn^{2+} and Mg^{2+} can act as allosteric regulators of ME and several other metabolic enzymes we supplemented our assay buffer with 1 mM $MnCl_2$ (Chou et al., 1998; Fedøy et al., 2007; Mildvan et al., 1966). As expected, the abundance of the M6 citrate isotopologues was now strongly increased indicating a Mn^{2+} dependent activation of ME (Fig. 3E). This result emphasizes that the composition of the buffer system has to be carefully monitored and adapted to the respective biological question to be studied.

The presented experiments highlight how the activity of mitochondrial metabolic enzymes dramatically changes with varying substrate availability. We showed that anaplerotic enzymes such as PC and ME are either activated or inhibited depending on pyruvate and glutamine supply to ensure sufficient ATP production. Notably, the ^{13}C-isotopes of the applied tracers were incorporated into the mitochondrial metabolite pool within only a few minutes and in the absence of ADP. This metabolic activity might be driven by either proton leak across the inner mitochondrial membrane or residual ATPase activity of remaining cytoplasmic enzymes. Although these results were obtained under *in situ* conditions, they strongly suggest that mitochondrial metabolism is also tightly regulated by cytosolic substrate supply *in vivo* regarding both the activity of individual enzymes and absolute fluxes.

It is interesting to note that during the timecourse experiments the abundance of individual isotopologues changed rapidly in the first minutes of the assay. These changes continuously decreased over time, which led us to the question whether mitochondria were reaching a metabolic steady-state or slowly lost their activity. To address this issue we performed an experiment with [U-^{13}C]pyruvate and glutamine as substrates. After 15 min of incubation we replaced the substrate solution by a buffer containing unlabeled pyruvate and glutamine instead of labeled pyruvate. After 30 min we performed a second substrate change back to the initial buffer containing the [U-^{13}C] pyruvate tracer. The corresponding fractional ^{13}C-carbon contribution of citrate is depicted in Fig. 3F. After 15 min of incubation 23% of the citrate carbon atoms were ^{13}C-labeled. This value increased to 27% within the following 15 min when the medium was not exchanged. If we however, replaced the buffer with buffer containing unlabeled pyruvate instead of [U-^{13}C]pyruvate almost no ^{13}C-isotopes were detected after 30 min (< 1%). The relative amount of ^{13}C-isotopes in citrate increased again to 24% within 15 min after we changed the medium back to the initial medium. This result clearly shows that mitochondria in selectively permeabilized cells do not only remain metabolically active, but also maintain the same level of activity for at least 45 min using the presented setup. Accordingly, we conclude that the dynamics observed during the time-resolved measurements are due to a metabolic steady state rather than a loss of mitochondrial activity.

3.3. Perturbation of mitochondrial metabolism using chemical effectors

3.3.1. ADP/GDP

In a next step, we evaluated whether the developed method was suitable to monitor metabolic changes caused by different biological perturbations. These perturbations were induced by directly treating *in situ* mitochondria with chemical effectors. The advantage of this approach as compared to intact cells is that mitochondrial enzyme activity can be assessed without secondary effects induced by cytosolic components. We decided to use an incubation time of 15 min rather than waiting for steady state conditions, to be able to detect changes in metabolic dynamics before reaching steady state conditions. One commonly applied means of stimulating mitochondrial respiration is the addition of ADP and GDP. We added both diphosphates directly to *in situ* mitochondria of A549 cells with [U-^{13}C]glutamine and unlabeled pyruvate as substrates. The application of a [U-^{13}C]glutamine tracer allows for the analysis of TCA cycle activity. The derived data represent a valuable addition to data on mitochondrial oxygen consumption, since they yield information on the activity of the underlying metabolic reactions.

During the first round of the TCA cycle M4 citrate is formed from [U-^{13}C]glutamine and unlabeled pyruvate. Further cycling leads to the emergence of the M2 (2nd round) and M1 isotopologues (3rd round). A slight increase of the M4 citrate isotopologue from 49% to 54% indicated a higher oxidative TCA cycle flux from glutamine to citrate after ADP supplementation (Fig. 4A). This came along with a more prominent increase in the cycling products M1 (from 1% to 5%) and M2 citrate (from 6% to 16%) and a decrease in the unlabeled (M0) fraction of citrate by 15% all indicating a highly increased cycling flux. These changes might seem relatively small as compared to the increase in oxygen uptake rate upon ADP stimulation. However, MIDs do not give information on absolute metabolic fluxes but rather contain information on relative isotopologue abundance, which is directly linked to the activities of the pathways producing a given metabolite.

We further observed increased uptake of both glutamine and pyruvate as well as increased glutamate secretion in ADP/GDP stimulated mitochondria, validating the isotope labeling data (Suppl. Fig. S4). Interestingly, absolute citrate levels increased by 75% upon

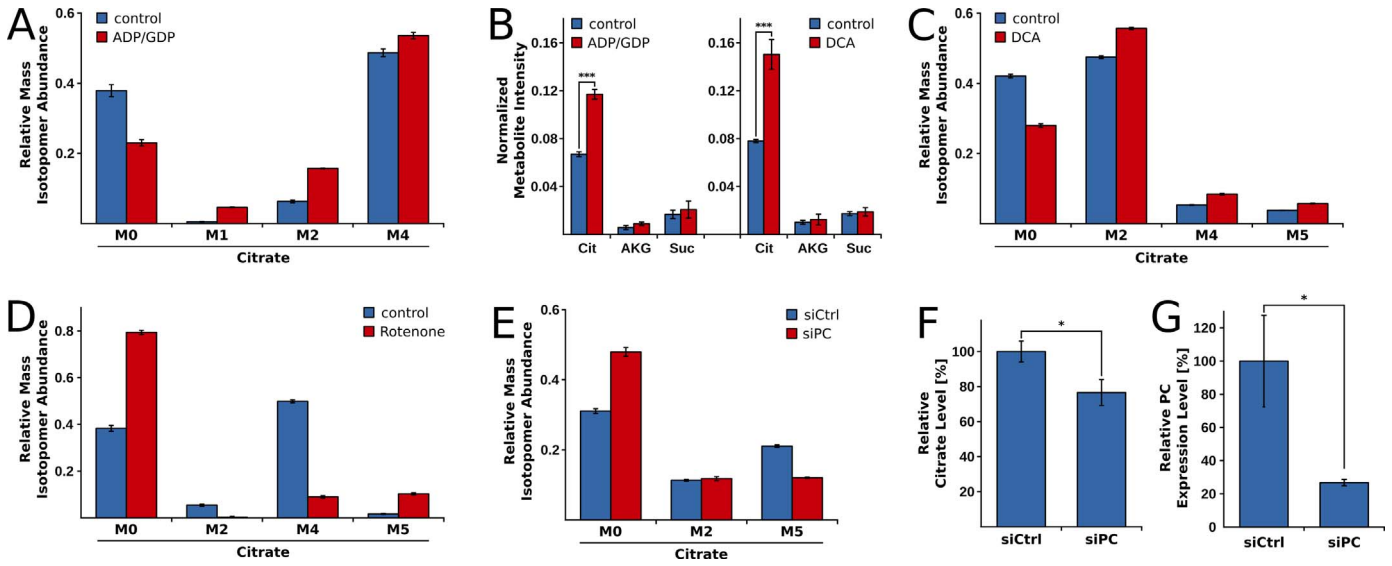

Fig. 4. Analysis of metabolic changes in selectively permeabilized A549 cells induced by chemical or genetic perturbation. (A) Relative abundance of the M0, M1, M2, and M4 citrate isotopologues after incubation with [U-^{13}C]glutamine and unlabeled pyruvate for 15 min. *In situ* mitochondria were treated with 2 mM ADP and 0.5 mM GDP for the duration of the assay. (B) Normalized metabolite intensities of citrate, α-ketoglutarate and succinate after incubation with [U-^{13}C]glutamine and unlabeled pyruvate for 15 min. *In situ* mitochondria were treated with either 2 mM ADP and 0.5 mM GDP (left) or 5 mM DCA (right) for the duration of the assay. (C) Relative abundance of the M0, M2, M4, and M5 citrate isotopologues after incubation with [U-^{13}C]pyruvate and unlabeled glutamine for 15 min. *In situ* mitochondria were treated with 5 mM DCA for the duration of the assay. (D) Relative abundance of the M0, M2, M4, and M5 citrate isotopologues after incubation with [U-^{13}C]glutamine and unlabeled pyruvate for 15 min. *In situ* mitochondria were treated with 1 μM rotenone for the duration of the assay. (E) Relative abundance of the M0, M2, and M5 citrate isotopologues after incubation with [U-^{13}C]pyruvate for 15 min. Cells were transfected with siRNA targeting pyruvate carboxylase 48 h prior to the assay. (F) Relative levels of citrate after incubation with [U-^{13}C]pyruvate for 15 min. Cells were transfected with siRNA targeting pyruvate carboxylase 48 h prior to the assay. (G) Relative expression levels of pyruvate carboxylase mRNA after treatment with non-targeted and PC siRNA. Bars indicate mean values and SD of n=3 for all figures, asterisks indicate p-values as determined using a Student's *t*-test: *p < 0.05, **p < 0.01, ***p < 0.001.

GDP/ADP treatment (Fig. 4B). While this is in line with the observed increase in TCA cycle activity it also suggests that citrate accumulates, likely due to a rate limiting step downstream of citrate synthase (CS). We suggest that the rate-limiting enzyme is isocitrate dehydrogenase 2 or 3 (IDH2/3) since the levels of AKG and succinate remained unchanged (Fig. 4B). IDH2 and 3 are subject to feedback inhibition *via* ATP and NAD(P)H and have already been identified as important rate controlling enzymes in earlier studies (Wahrheit et al., 2015; Williamson and Cooper, 1980).

3.3.2. Dichloroacetic acid

Another alternative of perturbing mitochondrial carbon flux is the stimulation with dichloroacetic acid (DCA). DCA has gained attention in recent years as a potential anti-cancer drug due to its ability to inhibit pyruvate dehydrogenase kinase (Michelakis et al., 2008). Inhibition of PDK leads to activation of its target PDH which in turn induces enhanced coupling of glycolysis and TCA cycle, and thus, reduced lactate production. To test whether we are able to assess this effect using the presented method, we subjected digitonin-permeabilized A549 cells to DCA. We used [U-^{13}C]pyruvate together with unlabeled glutamine to profile PDH activity and subsequent TCA cycle metabolism in digitonin-permeabilized A549 cells. As shown earlier in this study, PDH activity leads to the production of M2 citrate. Metabolic cycling of M2 citrate isotopologues produces M4 citrate, whereas the M5 citrate isotopologue is formed by PC activity as described earlier.

As expected, we observed an increase in the M2 citrate isotopologue from 48% to 56%, which is indicative of an enhanced PDH flux (Fig. 4C). The cycling-derived M4 isotopologue also increased from 5% to 8%, suggesting increased TCA cycle activity. Apparently, PDH activation elevated acetyl-CoA levels sufficiently to cause activation of PC (increased M5 citrate) even in the presence of glutamine-derived oxaloacetate. Similar to the stimulation with ADP, citrate levels were markedly increased upon DCA treatment (193% of control; Fig. 4B). Levels of AKG and succinate remained unchanged, again suggesting an accumulation of citrate with IDH2 being the rate-limiting step. It should be noted that the described metabolic effects occurred within only 15 min after the addition of DCA. This is even more remarkable, given the fact that DCA only indirectly affects PDH *via* inhibition of PDK. When we performed the same experiment in the presence of ADP, the effect of DCA was less pronounced, indicating that ADP stimulated mitochondria are already running on almost full capacity (Suppl. Fig. S5). These results highlight how fast mitochondria can adapt metabolic fluxes as a means to cope with a dynamic environment.

3.3.3. Rotenone

In contrast to stimulating mitochondrial activity using ADP/GDP or DCA we also analyzed the effect of complex I (NADH:ubiquinone reductase) inhibition on mitochondrial metabolism. We induced inhibition of complex I by the addition of rotenone directly to *in situ* mitochondria in the presence of [U-^{13}C]glutamine and unlabeled pyruvate. While oxidative TCA cycle metabolism on these substrates mainly generates M4 and M2 citrate isotopologues (see above), M5 citrate can be formed by IDH-mediated reductive carboxylation of [U-^{13}C]glutamine derived AKG. Under control conditions 5% and 50% of citrate were M2 and M4 labeled, respectively after 15 min of incubation (Fig. 4D). Only less than 2% of the citrate pool consisted of M5 isotopologues. When we performed the incubation in the presence of 1 μM rotenone, the M4 fraction was reduced to 9%, whereas the M2 isotopologues disappeared completely. The abundance of M5 isotopologues, however increased to 10%. The overall amount of ^{13}C-labeled isotopomers was decreased, as indicated by an increase in unlabeled (M0) citrate from 38% to 79%. The decrease in both the M2 and M4 isotopologue indicates decreased oxidative TCA cycle metabolism. This might be due to the lack of the cofactor NAD^+ which can not be recovered from NADH at complex I anymore. Since NAD^+ is necessary to maintain an oxidative TCA cycle, these fluxes are decreased upon rotenone treatment. Reductive carboxylation of AKG to isocitrate/citrate, as reflected in the increase in M5 citrate, might be activated to produce $NADP^+$ and ensure sufficient citrate production for fatty acid synthesis *in vivo* (Mullen et al., 2012). While it has not yet been fully elucidated which isoform of IDH is mainly responsible for

reductive carboxylation *in vivo*, (*e.g.* during mitochondrial dysfunction or hypoxic conditions) we were able to show that IDH2 is capable of taking that role at least during artificial ETC inhibition. Although theoretically possible, reductive carboxylation through IDH3 is unlikely, since previous studies found that this isoform is not able to catalyze the conversion of alpha-ketoglutarate to isocitrate (Mullen et al., 2012).

3.4. Perturbation of mitochondrial metabolism using RNAi

In a further experiment we intended to show that we are able to apply the developed setup to detect metabolic changes in cells with varying transcriptional activity. We chose PC as a target, because (i) it has been shown to play a vital role in the glutamine independent growth of cancer cells (Cheng et al., 2011) and (ii) it is activated in A549 mitochondria upon glutamine limitation (Fig. 3C). We applied siRNA targeting pyruvate carboxylase to A549 cells to decrease the expression of this enzyme 48 h prior to performing the assay. PC expression was decreased by 75% compared to the control as determined by qPCR (Fig. 4G). We used [U-^{13}C]pyruvate as the only substrate during the mitochondrial assay, since we observed activation of PC under these conditions. Analysis of the citrate mass isotopomer distribution revealed that the unlabeled fraction increased from 31% to 48% upon PC knockdown (Fig. 4E). The relative amount of the M2 isotopologue, which is formed during the condensation of unlabeled oxaloacetate from an endogenous pool with [U-^{13}C]pyruvate-derived acetyl-CoA, remained constant (11%). In contrast, the abundance of the PC-derived M5 citrate isotopologue dropped from 21% to 12%. The abundances of the cycling products derived from M5 citrate (M4 and M6 citrate) also decreased upon PC knockdown (Suppl. Table S3). Overall citrate levels were decreased by 25% relative to the control (Fig. 4F). The constant levels of M2 citrate show that PDH flux was still active even when PC expression was inhibited. As soon as the mitochondrial oxaloacetate pool is depleted, acetyl-CoA accumulates and PC is activated. Since this was only possible to a limited extent due to the PC knockdown, we observed a decrease in M5 citrate. The decrease in the overall citrate level shows that mitochondria can not compensate for lost PC activity, *e.g.* by reverse ME2 flux. Although the knockdown was not fully efficient, the decrease in PC expression was sufficient to detect the induced metabolic changes. The observed results indicate that the presented setup is well-suited to monitor metabolic changes in mitochondria induced by varying gene expression of metabolic enzymes.

4. Conclusions

In the presented study we developed a method for the targeted analysis of mitochondrial metabolism which combines selective permeabilization with stable isotope assisted metabolomics. Mitochondria inside of digitonin-permeabilized cell ghosts maintained an active membrane potential and exhibited respiratory activity for at least 45 min. Mitochondrial respiration was both stimulated and inhibited by the addition of respective effectors, indicating that mitochondria remained in a physiologically active state. Using uniformly ^{13}C-labeled glutamine and pyruvate tracers we could demonstrate how mitochondrial fluxes change in order to adapt to substrate and cofactor availability as well as chemical and transcriptional perturbations. These changes occurred within only a few minutes, highlighting that mitochondria are highly dynamic and versatile metabolic actors. The developed method provides means of shedding light on mitochondrial metabolism and adds valuable information to the analysis of compartmentalized, mammalian cell models. Potential applications include (i) the identification of metabolic bottlenecks or rate-limiting steps inside the mitochondria, (ii) screening for compounds directly acting on mitochondria, (iii) screening for cells carrying mutations in mitochondria-related genes, (iv) elucidation of the localization of metabolic enzymes and (v) identification of mitochondrial metabolite transporters.

Author contributions

YN, AW and KH conceived the project. YN, AW, RP, AFdH, AS, MNS, LK, FC and KH designed the experiments. YN, AW, RP, AFdH, MNS, FC and LK performed the experiments and data analysis. YN, AW and KH wrote the manuscript.

Acknowledgements

The authors want to thank the Metabolomics group at the LCSB for fruitful discussions and feedback. We would also like to thank Christian Jäger of the LCSB Metabolomics Platform for developing GC-MS methods and providing analytical support. This research was funded by the Fonds National de la Recherche (FNR) Luxembourg (ATTRACT A10/03 and THActivity CORE).

Appendix A. Supplementary material

Supplementary material associated with this article can be found in the online version at http://dx.doi.org/10.1016/j.ymben.2016.12.005.

References

Abe, Y., Sakairi, T., Kajiyama, H., Shrivastav, S., Beeson, C., Kopp, J.B., 2010. Bioenergetic characterization of mouse podocytes. Am. J. Physiol.: Cell Physiol. 299, C464–C476.
Antoniewicz, M.R., 2015. Methods and advances in metabolic flux analysis: a mini-review. J. Ind. Microbiol. Biotechnol. 42, 317–325.
Battello, N., Zimmer, A.D., Goebel, C., Dong, X., Behrmann, I., Haan, C., Hiller, K., Wegner, A., 2016. The role of HIF-1 in oncostatin M-dependent metabolic reprogramming of hepatic cells. Cancer Metab. 4, 3.
Cheng, T., Sudderth, J., Yang, C., Mullen, A.R., Jin, E.S., Matés, J.M., DeBerardinis, R.J., 2011. Pyruvate carboxylase is required for glutamine-independent growth of tumor cells. Proc. Natl. Acad. Sci. USA 108, 8674–8679.
Chou, W.Y., Huang, S.M., Chang, G.G., 1998. Conformational stability of the N-terminal amino acid residues of mutated recombinant pigeon liver malic enzymes. Protein Eng. 11, 371–376.
Clayton, D.A., Shadel, G.S., 2014. Isolation of mitochondria from tissue culture cells. Cold Spring Harb. Protoc. 2014, (pdb.prot080002).
Fedøy, A.-E., Yang, N., Martinez, A., Leiros, H.-K.S., Steen, I.H., 2007. Structural and functional properties of isocitrate dehydrogenase from the psychrophilic bacterium desulfotalea psychrophila reveal a cold-active enzyme with an unusual high thermal stability. J. Mol. Biol. 372, 130–149.
Fiskum, G., Craig, S.W., Decker, G.L., Lehninger, A.L., 1980. The cytoskeleton of digitonin-treated rat hepatocytes. Proc. Natl. Acad. Sci. USA 77, 3430–3434.
Gravel, S.-P., Andrzejewski, S., Avizonis, D., St-Pierre, J., 2014. Stable isotope tracer analysis in isolated mitochondria from mammalian systems. Metabolites 4, 166–183.
Hafner, R.P., Brown, G.C., Brand, M.D., 1990. Analysis of the control of respiration rate, phosphorylation rate, proton leak rate and protonmotive force in isolated mitochondria using the “top-down” approach of metabolic control theory. Eur. J. Biochem. 188, 313–319.
Heggeness, M.H., Simon, M., Singer, S.J., 1978. Association of mitochondria with microtubules in cultured cells. Proc. Natl. Acad. Sci. USA 75, 3863–3866.
Hiller, K., Hangebrauk, J., Jäger, C., Spura, J., Schreiber, K., Schomburg, D., 2009. MetaboliteDetector: comprehensive analysis tool for targeted and nontargeted GC/MS based metabolome analysis. Anal. Chem. 81, 3429–3439.
Holian, A., Owen, C.S., Wilson, D.F., 1977. Control of respiration in isolated mitochondria: quantitative evaluation of the dependence of respiratory rates on [ATP], [ADP], and [Pi]. Arch. Biochem. Biophys. 181, 164–171.
Jitrapakdee, S., St Maurice, M., Rayment, I., Cleland, W.W., Wallace, J.C., Attwood, P.V., 2008. Structure, mechanism and regulation of pyruvate carboxylase. Biochem. J. 413, 369–387.
Klein, S., Heinzle, E., 2012. Isotope labeling experiments in metabolomics and fluxomics. Wiley Interdiscip. Rev. Syst. Biol. Med. 4, 261–272.
Krysko, D.V., Agostinis, P., Krysko, O., Garg, A.D., Bachert, C., Lambrecht, B.N., Vandenabeele, P., 2011. Emerging role of damage-associated molecular patterns derived from mitochondria in inflammation. Trends Immunol. 32, 157–164.
Lewis, C.A., Parker, S.J., Fiske, B.P., McCloskey, D., Gui, D.Y., Green, C.R., Vokes, N.I., Feist, A.M., Heiden, M.G.V., Metallo, C.M., 2014. Tracing compartmentalized NADPH metabolism in the cytosol and mitochondria of mammalian cells. Mol. Cell 55, 253–263.
Lin, M.T., Beal, M.F., 2006. Mitochondrial dysfunction and oxidative stress in neurodegenerative diseases. Nature 443, 787–795.
Manor, U., Bartholomew, S., Golani, G., Christenson, E., Kozlov, M., Higgs, H., Spudich,

J., Lippincott-Schwartz, J., 2015. A mitochondria-anchored isoform of the actin-nucleating spire protein regulates mitochondrial division. eLife 4, e08828.
van Meer, G., Voelker, D.R., Feigenson, G.W., 2008. Membrane lipids: where they are and how they behave. Nat. Rev. Mol. Cell Biol. 9, 112–124.
Michelakis, E.D., Webster, L., Mackey, J.R., 2008. Dichloroacetate (DCA) as a potential metabolic-targeting therapy for cancer. Br. J. Cancer 99, 989–994.
Mildvan, A.S., Scrutton, M.C., Utter, M.F., 1966. Pyruvate carboxylase VII. A possible role for tightly bound manganese. J. Biol. Chem. 241, 3488–3498.
Modica-Napolitano, J.S., Singh, K.K., 2004. Mitochondrial dysfunction in cancer. Mitochondrion 4, 755–762.
Mullen, A.R., Wheaton, W.W., Jin, E.S., Chen, P.-H., Sullivan, L.B., Cheng, T., Yang, Y., Linehan, W.M., Chandel, N.S., DeBerardinis, R.J., 2012. Reductive carboxylation supports growth in tumour cells with defective mitochondria. Nature 481, 385–388.
Murphy, M.P., 2009. How mitochondria produce reactive oxygen species. Biochem. J. 417, 1–13.
Nicolae, A., Wahrheit, J., Nonnenmacher, Y., Weyler, C., Heinzle, E., 2015. Identification of active elementary flux modes in mitochondria using selectively permeabilized CHO cells. Metab. Eng. 32, 95–105.
Niedenführ, S., Wiechert, W., Nöh, K., 2015. How to measure metabolic fluxes: a taxonomic guide for 13C fluxomics. Curr. Opin. Biotechnol. 34, 82–90.
Palmieri, F., Pierri, C.L., 2010. Mitochondrial metabolite transport. Essays Biochem. 47, 37–52.
Rogers, G.W., Brand, M.D., Petrosyan, S., Ashok, D., Elorza, A.A., Ferrick, D.A., Murphy, A.N., 2011. High throughput microplate respiratory measurements using minimal quantities of isolated mitochondria. PLOS ONE 6, e21746.
Salabei, J.K., Gibb, A.A., Hill, B.G., 2014. Comprehensive measurement of respiratory activity in permeabilized cells using extracellular flux analysis. Nat. Protoc. 9, 421–438.
Schulz, I., 1990. Permeabilizing cells: some methods and applications for the study of intracellular processes. Methods Enzymol. 192, 280–300.
Silva, A., Oliveira, P., 2012. Evaluation of respiration with clark type electrode in isolated mitochondria and permeabilized animal cells. In: Palmeira, C.M., Moreno, A.J. (Eds.), Mitochondrial Bioenergetics. Humana Press, 7–24.
Stepanova, A., Shurubor, Y., Valsecchi, F., Manfredi, G., Galkin, A., 2016. Differential susceptibility of mitochondrial complex II to inhibition by oxaloacetate in brain and heart. Biochim. Biophys. Acta BBA: Bioenerg. 1857, 1561–1568.
Vacanti, N.M., Divakaruni, A.S., Green, C.R., Parker, S.J., Henry, R.R., Ciaraldi, T.P., Murphy, A.N., Metallo, C.M., 2014. Regulation of substrate utilization by the mitochondrial pyruvate carrier. Mol. Cell 56, 425–435.
Wahrheit, J., Nonnenmacher, Y., Sperber, S., Heinzle, E., 2015. High-throughput respiration screening of single mitochondrial substrates using permeabilized CHO cells highlights control of mitochondria metabolism. Eng. Life Sci. 15, 184–194.
Wegner, A., Weindl, D., Jäger, C., Sapcariu, S.C., Dong, X., Stephanopoulos, G., Hiller, K., 2014. Fragment formula calculator (FFC): determination of chemical formulas for fragment ions in mass spectrometric data. Anal. Chem. 86, 2221–2228.
Wegner, A., Meiser, J., Weindl, D., Hiller, K., 2015. How metabolites modulate metabolic flux. Curr. Opin. Biotechnol. 34, 16–22.
Wiechert, W., 2001. 13C metabolic flux analysis. Metab. Eng. 3, 195–206.
Williamson, J.R., Cooper, R.H., 1980. Regulation of the citric acid cycle in mammalian systems. FEBS Lett. 117, K73–K85.
Wong, R., Steenbergen, C., Murphy, E., 2012. Mitochondrial permeability transition pore and calcium handling. Methods Mol. Biol. 810, 235–242.
Yang, C., Ko, B., Hensley, C.T., Jiang, L., Wasti, A.T., Kim, J., Sudderth, J., Calvaruso, M.A., Lumata, L., Mitsche, M., et al., 2014. Glutamine oxidation maintains the TCA cycle and cell survival during impaired mitochondrial pyruvate transport. Mol. Cell 56, 414–424.
Yao, J., Irwin, R.W., Zhao, L., Nilsen, J., Hamilton, R.T., Brinton, R.D., 2009. Mitochondrial bioenergetic deficit precedes Alzheimer's pathology in female mouse model of Alzheimer's disease. Proc. Natl. Acad. Sci. USA 106, 14670–14675.